Progress in Nuclear Energy 172 (2024) 105186

Contents lists available at ScienceDirect

Progress in Nuclear Energy

journal homepage: www.elsevier.com/locate/pnucene

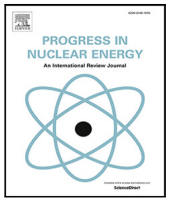

Modeling gamma detectors in OpenMC: Validation of a newly implemented pulse-height tally

Christopher Fichtlscherer [a,b], Milon Miah [c], Friederike Frieß [d], Malte Göttsche [b,*], Moritz Kütt [a]

[a] Institute for Peace Research and Security Policy at the University of Hamburg, Beim Schlump 83, 20144 Hamburg, Germany
[b] Nuclear Verification and Disarmament Group, Physics Institute III B, RWTH Aachen University, Schinkelstr. 2, 52062 Aachen, Germany
[c] Heidelberg University, Grabengasse 1, 69117 Heidelberg, Germany
[d] University of Natural Resources and Life Sciences, Vienna, Department of Water, Atmosphere, and Environment, Institute of Safety and Risk Sciences, Peter-Jordan-Straße 76/1, 1190 Vienna, Austria

ARTICLE INFO

Keywords:
Detector modeling
OpenMC
Pulse height tally
Code development
Code validation
Monte carlo particle transport code

ABSTRACT

Gamma spectroscopy measurements can be simulated using a pulse-height tally functionality of Monte Carlo particle transport codes. Such a functionality must account for the complete simulation history of a particle's energy deposited in a particular volume. OpenMC, an open-source application for neutron and photon particle transport which is widely used in the nuclear engineering community, previously lacked adequate simulation capabilities for gamma spectroscopy. In this paper, we outline the implementation of the photon pulse-height tally for OpenMC. Additionally, we validate the new function by comparing results to analytical calculations, other software, and experimental data.

1. Introduction

The examination of radioactive substances is commonly conducted through the application of gamma spectroscopy. This includes, for example, environmental monitoring, the characterization of radioactive waste, nuclear security applications like the authentication of nuclear weapons or the characterization of uranium enrichment or geophysical applications that include well-logging and determination of surface compositions (cf. Carminati et al. (2022), Carasco (2021), Kütt and Glaser (2019), Nguyen and Zsigrai (2006), Jeon et al. (2020), and Prettyman et al. (2006)). Simulation of measurement outcomes is necessary for the development of new applications, optimization of detectors and for the detailed analysis of the measured results.

Deterministic approaches such as used within GADRAS-DRF (Horne et al., 2016) allow for very precise calculations of the detector response but are limited to relatively simple detector geometries. There exist several established codes to determine the response function of a detector that use Monte Carlo particle transport methods. Examples are MCNP6.2 (Werner et al., 2018), GEANT4 (Agostinelli et al., 2003), FLUKA (Böhlen et al., 2014; Ferrari et al., 2005), EGSnrc (Kawrakow et al., 2021), EGS5 (Hirayama et al., 2015), PENELOPE (Salvat et al., 2009), MCSHAPE (Scot and Fernandez, 2015), MARTHA (Saito and Moriuchi, 1981), or SIMSPEC-G (Nayak and Mukherjee, 2022). These codes usually use pulse-height tallies (PHT) to measure the energy which is deposited in a given volume by gamma radiation. Under optimal conditions, the simulated output signal from the detector correlates proportionally with the energy.

All the listed code packages have limitations. Some are export-controlled (MCNP, GADRAS-DRF, and MARTHA), limiting access of a larger international community. Others are proprietary (FLUKA, PENELOPE), limiting transparency regarding underlying methods. Furthermore, certain tools are only designed for specific energy ranges (MCSHAPE and SIMSPEC-G). The two related open-source codes, EGS5 and EGSnrc, have their origins in accelerator physics and do not have the capability to model neutrons. Consequently, they cannot be used in nuclear engineering. GEANT4 is open source, but targets the user group of high-energy physicists, and is significantly slower than other codes. For example, simulation of a gamma spectrum as shown in Fig. 6 with 10^6 particles took 5.40 s with OpenMC and 44.60 s with Geant4-11.1.2 (running on a single *AMD Ryzen 7 PRO 6850U* core, excluding compilation time and averaging over 100 separate runs).

OpenMC, an efficient open-source Monte Carlo code, can be freely accessed under its MIT license (Romano et al., 2015). It is an actively developed and widely used code in the field of nuclear engineering. Initially, OpenMC develops concentrated their efforts on neutron transport. In 2018, they added the capacity to simulate photon transport (Lund and Romano, 2018). However, OpenMC was lacking the functionality of a Pulse-Height Tally (PHT). Interest for such a functionality exists within the user community. For example, El-Bouzaidi

* Corresponding author.
E-mail address: goettsche@nvd.rwth-aachen.de (M. Göttsche).

https://doi.org/10.1016/j.pnucene.2024.105186
Received 15 December 2023; Received in revised form 16 March 2024; Accepted 17 March 2024
Available online 1 April 2024

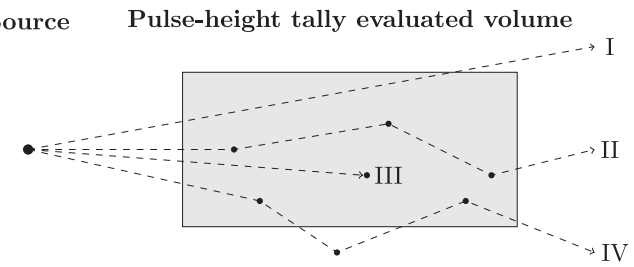

Fig. 1. Four illustrative particle histories are depicted in the figure, where points indicate the locations of interactions, and dashed lines represent the particle tracks. The same figure was used in Fichtlscherer et al. (2021).

et al. (2023) describe simulations to determine the response function of a sodium-iodide (NaI) detector with OpenMC. Albeit in principle similar to a PHT, the method described in El-Bouzaidi et al. (2023) lacks a key element, namely the proper accounting for particles undergoing software-based energy cutoff, leading to erroneous results.

This article details the integration and verification of a photon PHT.[1] This tally has recently been incorporated into the primary OpenMC code base, allowing for transparent and reproducible simulations of gamma spectroscopy measurements.

2. Implementation

To determine the Pulse-Height Tally (PHT) value, it is crucial to maintain a record of the overall energy deposited in a specified volume by both the incident photon and secondary particles generated through interactions with the detector material (e.g., photoelectric effect). Fig. 1 provides an illustration of four particle tracks: Particle I experiences no interactions within the detector volume, leading to a PHT value of zero. The PHT value for particle II can be obtained by summing up the energies lost during three scattering interactions. Particle III is fully absorbed in the volume through the photoelectric effect, resulting in the PHT value reflecting the particle's total energy. Particle IV's PHT value is determined by considering only the energies lost during two scattering reactions that occur within the volume.

For most unknown properties of a system, using tallies in Monte Carlo methods is an alternative way to solving the Boltzmann transport equations (Boltzmann, 1872; Booth, 1994). Typically, such tallies can be calculated on-the-fly by counting each reaction separately, regardless of the interacting particle's previous or subsequent interactions. By using large numbers of particles, it is possible to infer the underlying properties of the system. As an instance, the likelihood of a particle crossing a specific surface can be established using this approach. However, pulse-height tallies are non-Boltzmann tallies, meaning their value cannot be obtained by solving the Boltzmann transport equations. The value of the PHT depends on the effects of multiple interactions, including different particles (e.g., pair-production), necessitating more advanced implementation methods. Prior to evaluating the PHT value, it is necessary to simulate the entire history of the particle.

The capability to record energy deposited by individual particle interactions in a specific volume was enabled by introducing a new method to the `OpenMC::particle` class within OpenMC's object-oriented framework. This method allows for the determination of energy deposited by photons, which occurs through one of three primary interactions: Incoherent (Compton) scattering, photoelectric effect, or pair production. In addition to these interactions, the method accounts for any secondary photons generated and subtracts their energy from the PHT value. The interaction of photons with nuclides may also generate electrons or positrons as secondary particles. OpenMC is not capable of modeling these particles but employs the following approximations: First, instead of positrons, two isotropic 511 keV annihilation photons in opposite directions are modeled. Second, for electrons, a thick-target bremsstrahlung approximation is used, where electrons are not transported but instead instantly generate bremsstrahlung photons (Lund and Romano, 2018). The alternative OpenMC offers for electrons, where all energy is deposited at the point of particle creation, is not used here. Third, additional photons are produced in the process of atomic relaxation. Fig. 2 presents the implemented method for determining the pulse-height tally as pseudo code.

In OpenMC (like in most other Monte-Carlo particle transport codes, for example, EGSnrc, FLUKA, Geant4, MCNP, and Penelope), the cross section data provided for photon interaction assumes interaction with cold, neutral, and isolated atoms (Cullen et al., 1997). Cross sections for materials consisting of different elements are approximated by the density-weighted sum of the cross sections of the individual elements. OpenMC photon interaction is modeled for energies down to 1 keV and it terminates transport for photons with lower energies (Lund and Romano, 2018) (the manual of MCNP6.2 also describes a default cut-off value of 1 keV Werner et al., 2018). Treatment for lower energies is difficult, as the interactions not only depend on elemental properties, but are influenced by other effects like the molecular structure of a material. We ensure proper accounting for particles below the cut-off value by adding the remaining energy to the PHT value of the volume in which there transport simulation is terminated.

Fig. 3 shows a simple example of how the new OpenMC feature can be accessed via its Python API.[2]

3. Validation

We conducted comprehensive validation to ensure that our implementation produces accurate results. Similar to our previous conference presentation of preliminary work (Fichtlscherer et al., 2021), this includes an analytical method, the comparison of the tally's results to the simulation software MCNP6.2, and to experimental data. However, here we used a much more complex model for analytical validation and revisited ambiguities and errors in other publications on this method. The simulation-based validation is more comprehensive, including a discussion of x-ray effects. Finally, we used a more complex broadening function for the experimental validation, which leads, among other things, to the fact that the shape of the Compton edge can be simulated much better. Further, additional effects like annihilation photons from β^+ decays were modeled.

3.1. Analytic validation

The PHT can be determined analytically in simplified physical models. Such simplified models were first described in Shuttleworth (1994).[3] MCNP developers used this validation method for their PHT functionality (Sood et al., 2004). We performed an analytical validation of the most complex scenario described in Sood et al. (2004), the two-region detector (see Fig. 4). In the design, two cylindrical volumes, each having a length and radius of $\ln(2)$ cm, are aligned sequentially. These

[1] An earlier version of this research is available in Fichtlscherer et al. (2021). The current paper offers a more comprehensive validation and integrates several technical improvements and describes the code as implemented in OpenMC.

[2] The full example is available at https://github.com/openmc-dev/openmc-notebooks/blob/main/gamma-detector.ipynb.

[3] Two publications with similar author groups give different results for the analytical validation of the PHT (Sood et al., 2003, 2004). Our values for the simplified model agree with the older one (Sood et al., 2003), in which the complex model is not discussed. The newer publication (Sood et al., 2004) contains values inconsistent with the previous publication for the simplified model. Very likely, the same source of inconsistency applies to the complex model, hence we provide new results here.

```
Require: a volume of concern ("pulse-height-volume", PHV)
initialize result with zero
while list of starting and secondary particles not empty do
    if photon-energy < cutoff-energy then
        if photon in PHV then
            result += photon-energy
        end if
        remove photon from list of starting and secondary particles
        skip to next iteration (line 2)
    end if
    start photon
    while photon alive do
        transport photon
        if photon reacts then
            add created particles to secondary particles
            if photon in PHV then
                dif = energy-before-reaction - energy-after-reaction
                result += dif
                for each newly created photon in secondary particles do
                    result -= photon-energy
                end for
            end if
        end if
        if photon-energy < cutoff-energy then
            if photon in PHV then
                result += photon-energy
            end if
            set photon alive to 0 ("kill")
        end if
    end while
    remove photon from list of starting and secondary particles
end while
```

Fig. 2. Pseudo-code representation of the determination of the pulse-height tally in OpenMC for a single cell. The actual implementation can be used for multiple detector volumes.

```python
tallies = openmc.Tallies()

energy_bins = np.linspace(0, 1e6, 1001)
energy_filter = openmc.EnergyFilter(energy_bins)
cell_filter = openmc.CellFilter(sodium_iodide_crystal)

tally = openmc.Tally(name='pulse-height')
tally.filters = [cell_filter, energy_filter]
tally.scores = ['pulse-height']

tallies.append(tally)
tallies.export_to_xml()
```

Fig. 3. Simple example of the pulse-height tally for a NaI scintillation detector via the OpenMC Python API.

cylinders are composed of three hypothetical elements: Kneeon (50%), Moron (20%), and Odium (30%). These hypothetical elements are used to represent simplified versions of pair production, photoelectric absorption, and Compton scattering interactions. Specifically, during the simplified pair production process, two photons are generated, each carrying a quarter of the energy of the incoming photon. If the energy of the incoming photon exceeds 1.0 MeV, one of the photons generated in the simplified pair production is scattered at an angle of ninety degrees. In the case of simplified Compton scattering, the photon loses half of its energy but maintains its original direction. For the simplified model of the photoelectric effect, the incoming particle is absorbed. The starting photons have an initial energy of 3.2 MeV and fly towards the first cylinder. They are absorbed within the volume once their energy drops below the 0.15 MeV threshold. The material of the cylinders possesses a total macroscopic cross section of 1 cm^{-1}. After the photons pass the first cylindrical volume, their pulse-height is determined in the second cylinder (marked in darker gray in Fig. 4). This scenario leads to 500 different particle histories, in which the PHT can take sixteen different values. The detailed calculations for analytical validations of the PHT can be found in Miah (2022). We modified the OpenMC source code

Table 1
This table shows the analytic and OpenMC simulation results for the different energies the PHT can take in the two-region setup. Further, the OpenMC-simulated PHT results together with the standard deviation σ of 100 sub-samples with 10^7 particles each per data point are given. The results are correlated.

Energy [MeV]	Analytic PHT result	OpenMC PHT result	σ	Energy [MeV]	Analytic PHT result	OpenMC PHT result	σ
0.0	0.561329	0.561327	0.000130	1.6	0.109465	0.109470	0.000098
0.2	0.023769	0.023769	0.000051	2.0	0.030379	0.030379	0.000052
0.4	0.063021	0.063027	0.000084	2.2	0.012559	0.012559	0.000035
0.6	0.019769	0.019778	0.000044	2.4	0.034298	0.034290	0.000056
0.8	0.049945	0.049950	0.000068	2.6	0.005003	0.005001	0.000024
1.0	0.002810	0.002810	0.000015	2.8	0.012088	0.012084	0.000036
1.2	0.013011	0.013008	0.000032	3.0	0.002873	0.002871	0.000018
1.4	0.002189	0.002189	0.000015	3.2	0.057493	0.057490	0.000068

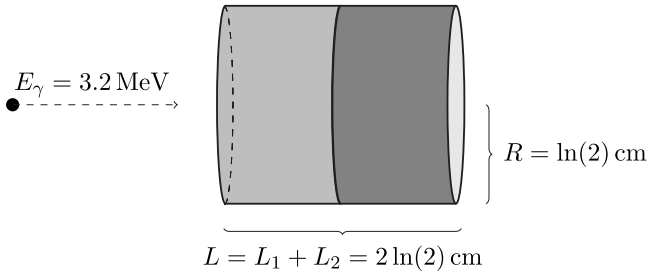

Fig. 4. The two-region detector implemented for the analytical validation of the PHT.

to model the simplified photon reactions for the actual validation. We ran an OpenMC simulation with 100 sub-samples of 10^7 particles each. Table 1 presents both the simulation and analytical outcomes, alongside the standard deviation σ of the simulated data.

One can observe that the simulated results agree with the expected analytical outcome within the statistical uncertainties.

3.2. Software-based validation

The results of identical PHT simulations in OpenMC 12.2 (Romano et al., 2015) and MCNP6.2 (Werner et al., 2018) were compared in the software-based validation. The detector design is derived from Mirion Technology's NaI-based "802 Scintillation Detector" (Mirion Technology Inc., 2017) (cf. Fig. 5). In the following, we modeled the back of the detector as a homogeneous aluminum block (Saito and Moriuchi, 1981; Tichacek et al., 2019). This material has a negligible impact on the final PHT outcome, as demonstrated by simulation results. All simulations were performed using the "Electron Photon Relaxation Data" 2014 (EPRDATA14) to model photon-related interactions. EPRDATA14 is a particular ACE data format for MCNP6.2, based on the IAEA's "Electron Photon Interaction Cross Sections" (EPICS) 2014 (Han et al., 2018). OpenMC data libraries are provided in HDF5 format and are based on common neutron-cross section evaluations. We use the OpenMC library ENDF/B-VII.1 from a set of Los Alamos National Laboratory-based data libraries. This library includes the EPRDATA14 for photon interactions (OpenMC, 2022). Both codes ran with an energy cutoff value of 1 keV and model the relevant physical interactions similar. Photons are started uniformly across a disk, mirroring the detector's radius with its casing, situated 10 cm ahead of the detector, and are projected directly towards the detector in a perpendicular orientation. Since the source has the same size as the entire detector, only 82 percent of the starting gamma particles will hit directly into the detector crystal. A fraction of the gammas missing the detector are scattered back into the crystal after interacting with the detector's casing. In MCNP, non-analog processes like knock-on electrons can generate negative PHT scores. Particles that just pass through the observed volume contribute an artificial value of 10^{-12} MeV to the PHT. Therefore, it is recommended to run MCNP with a zero bin and an additional epsilon bin at 10^{-5} MeV to separately account for both effects. In OpenMC, particles that do not pass through the volume do not contribute to the PHT. We ignore results from these first two bins, as they have no physical equivalent. Furthermore, in OpenMC, PHT values on the upper boundary of a bin are not counted in that bin, while this is the case in MCNP. Therefore, we have chosen the bins such that the epsilon bin is followed by 2048 equally sized bins, where the full-energy peak lies precisely in the middle of the uppermost bin. We have further shifted the OpenMC bins by 10^{-12} MeV to reduce the chance of other peaks falling exactly on the boundary. With an additional bin up to 20 MeV, we have checked that no unexpected counts of higher energies occur. We utilized the pulse-height functionality to simulate the measurement of this detector with various gamma sources and subsequently compared the obtained results.

Cs-137 spectrum. Fig. 6 shows simulation results for the scintillation detector described above with a starting photon energy of 0.6617 MeV (Cs-137). Each simulation included 10^{10} starting particles. The plot shows various characteristics, such as the full-energy peak (0.6617 MeV), the Compton edge (0.478 MeV), and the backscatter peak (0.184 MeV). At 33.2 keV (zoomed in), we see the so-called K-edge of iodine. There is a sudden rise in the likelihood of photoelectric absorption, corresponding to the binding energy of an iodine K-shell electron. This electron absorbs the energy of the photon during the absorption process. The two peaks next to each other (at 0.633 MeV) are the result of a photoelectric absorption and the subsequent escape of the K_α-(28 keV) or K_β-X-rays (31 keV) (Knoll, 2010). These characteristic X-rays are created when the vacancy in the inner K-shell is filled with an electron from the L- or the M-shell after the photoelectric absorption. Further, the differences between the escape of the $K_{\alpha,1}$ and the $K_{\alpha,2}$-X-rays or the $K_{\beta,1}$- and $K_{\beta,2}$-X-rays can be seen. The two tiny peaks in the Compton valley at 0.602 MeV (zoomed in) result from a double escape of the K_α- and K_β-X-rays. After the electron is forced out of the K-shell in the initial photoelectric absorption, the thick-target bremsstrahlung approximation is used to determine which photons are produced by the deceleration of the electron. These photons can have an energy higher than 33.2 keV and potentially lead to secondary photoelectric absorptions emitting K_α and K_β-X-rays, able to escape again. The two peaks represent this escape of two K_α-X-rays or one K_α- and one K_β-X-ray. The peak of the double K_β X-ray escape is not visible because of its statistically unlikely occurrence (the probability for an K_β X-ray escape is much lower than an K_α-X-ray escape). If only the crystal without surrounding material is simulated, the third peak becomes visible. The small, broadened peak to the right of the full-energy peak results from the escape of the L_α-X-rays after photoelectric absorption.

In the lower part of Fig. 6, we have plotted the relative error. The most significant differences are discernible for very small energies at the K-edge of iodine and the bins directly to the left of the full-energy peak. In spite of these variations, the two spectra exhibit a high degree of similarity overall. The two spectra's full-energy peak height differs by less than 0.05%. We conclude that our development provides a viable alternative to simulate a specific spectrum.

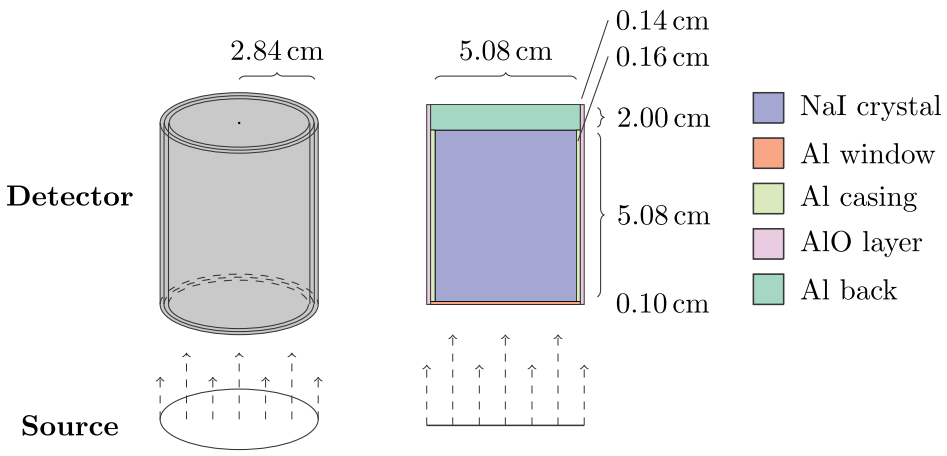

Fig. 5. The detector model employed for simulations in both OpenMC and MCNP6.2 is derived from the "802 Scintillation Detector" by Mirion Technology (Mirion Technology Inc., 2017). The same figure appeared in Fichtlscherer et al. (2021).

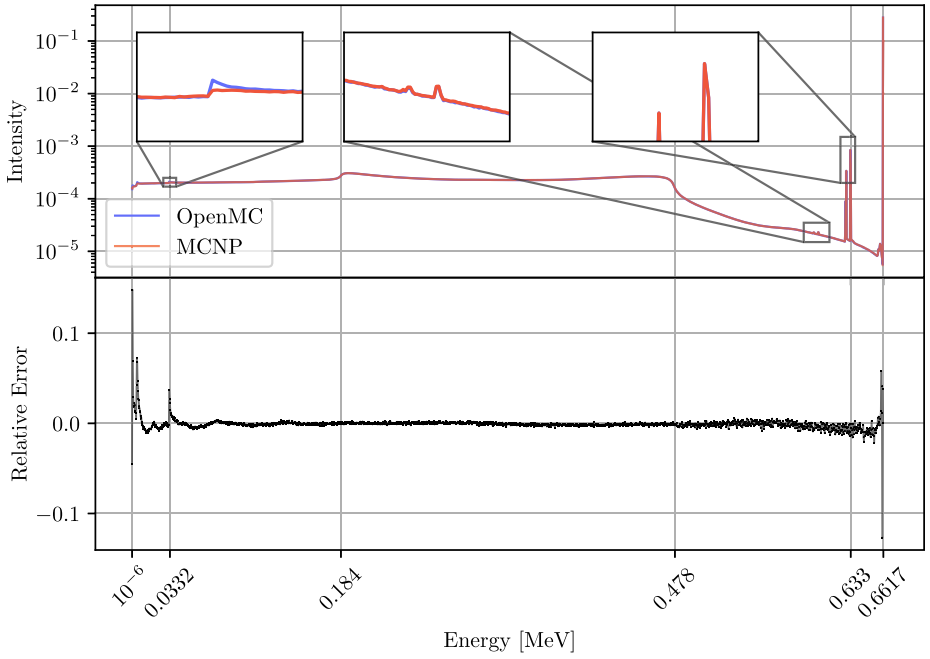

Fig. 6. The top plot displays the simulation results of measuring a Cs-137 gamma spectrum using a pulse-height tally in both OpenMC and MCNP6.2. The lower plot illustrates the relative error in these simulations.

Comparing various energies. A total of 295 simulations were conducted for photons with incoming energies ranging from 0.05 MeV to 3 MeV, in increments of 10 keV. Each simulation results in an individual spectrum with 2048 energy bins analogous to the Cs-137 spectrum described above. The simulations involved 10^8 initial particles for each run. The Kolmogorov–Smirnov test (Massey, 1951) was employed between all 295 energy levels for each pair of OpenMC and MCNP6.2 simulations. In this statistical test, the maximum norm between the cumulative function of the spectra is computed (H_0: both spectra follow the same probability distribution). If it surpasses the critical value

$$d_\alpha = c(\alpha) \cdot \sqrt{\frac{n_1 + n_2}{n_1 \cdot n_2}}, \tag{1}$$

where $c(\alpha)$ is the Kolmogorov distribution, n_1 and n_2 are the sample sizes, and H_0 is rejected at a significance level of α. The gamma spectra derived from the simulations were normalized to one, and we excluded the first energy bin's results to prevent double-counting. The first bin includes the number of particles that did not interact with the detector, which has no physical measurement equivalent. With $n_1 = n_2 = 2047$ and a significance level of $\alpha = 0.05$, the critical value is $d_\alpha = 0.03$.

For very small energies, we still see that the spectra differ more than for higher energies — yet they are well below the significance level of the Kolmogorov–Smirnov test. We find good similarity (low Kolmogorov–Smirnov test results) for most values. Initially, exceptions were visible for the energies of 1.45, 1.69, 1.93, 2.41, 2.68, and 2.84 MeV (shown in red in Fig. 7). Further investigation showed that a software error likely causes these differences in MCNP6.2. In each case, only two energy bins contained significantly different values because specific peaks (single-escape peak, double-escape peak, or photon annihilation peak) were registered in a wrong bin. This was the case when the peak's energy was within 10 eV of a bin border. Therefore, we repeated the simulations with bin borders shifted by 20 eV, which solves the issue (shown in blue in Fig. 7).

Overall, results are indicating a very good agreement between the newly implemented PHT and the tally functionalities of MCNP6.2.

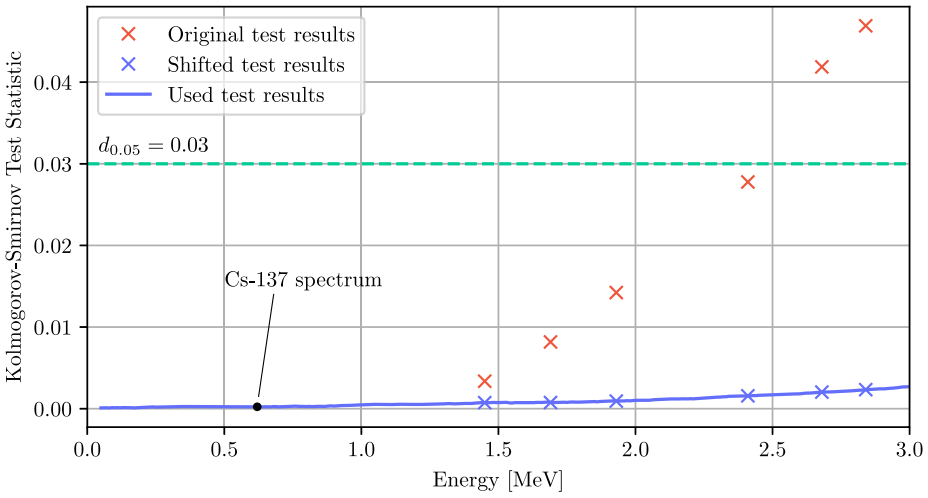

Fig. 7. A comparison of 295 spectra within the 0.05 MeV to 3 MeV energy range, generated by OpenMC and MCNP6.2, using the Kolmogorov–Smirnov test to determine if the simulation results conform to the same underlying probability distribution. The results are considered consistent at a significance level of $\alpha = 0.05$ if the test outcome is below the critical value d_α. Results are plotted as a line to improve visibility. Initially, MCNP6.2 pulse-height tally results for 1.45, 1.69, 1.93, 2.41, 2.68, and 2.84 MeV showed large discrepancies, because some events were sorted in incorrect bins (red). Using minimally shifted energy bins (20 eV), results improve significantly (blue).

3.3. Experimental validation

A comprehensive set of experimental measurements using a 3 × 3 inch NaI scintillation detector for different isotopic sources can be found in Heath (1964). The PHT functionality of OpenMC was used to simulate these measurements. The detector was conceptualized as a cylinder composed of sodium iodide, with thin layers of aluminum oxide and pure aluminum. An iron block was used to model the detector's back. As there is no specific details on the source and the background given, we assume isotopic point sources and neglect the background. As a result, the subsequent findings are primarily a qualitative comparison.

The effect of diverse physical phenomena, including charge collection statistics, electronic noise, and spatial variations in the detector response across its active volume, results in the broadening of peaks in experimental gamma spectra, rather than the appearance of narrow lines (Knoll, 2010). When the energies of incoming photons are in very close, the detector may register them as a single peak. This is described by the energy resolution of a detector, which characterizes its ability to differentiate closely spaced peaks. For a specific energy, the detector's resolution is defined as the ratio of the full width at half maximum (FWHM) of the full-energy peak to its energy. The standard deviation $\sigma(E)$ of the approximating distribution, for a given energy E, is by

$$\sigma(E) = \frac{\mathrm{FWHM}(E)}{2\sqrt{2\ln 2}} \tag{2}$$

is related to the FWHM of a peak with a specific energy. To determine the energy-dependent resolution of the detector, we perform a fit of the measured resolutions read manually from Figure 6 in Heath (1964) to the function

$$R(E) = \frac{\mathrm{FWHM}(E)}{E} = \frac{a + b\sqrt{E + cE^2}}{E} \tag{3}$$

Fig. 8 displays both the individual values and the fit, employing the parameters $a = -0.643$ MeV, $b = 6.794$ MeV$^{0.5}$ and $c = 0.258$ MeV^{-1}. with a mean squared error of the fitting of 0.219. The figure also shows detector resolutions calculated from the nine experiments presented below. The spectra we analyzed have, on average, a slightly worse resolution than the isotopes used to determine the detector's resolution. In our experimental simulation, we applied Gaussian broadening on the PHT results through an additional Python function, to mimic the characteristics observed in real experimental measurements (Knoll, 2010). Fig. 9 illustrates nine experimental measurements and their corresponding simulated spectra, with vertical lines indicating the original sources of photon energies. The energy and intensities of the gamma emissions of the radioactive isotopes were obtained from the Python package PyNE 0.7.1 — The Nuclear Engineering Toolkit (Bates et al., 2014). The total number of emitted photons of the respective source is given in Heath (1964).

For some experimental spectra, no absolute source activity was given, marked in Fig. 9. For comparison, the simulation results were normalized based on the total counts of the experiment. The detector efficiency provided in Heath (1964) was utilized for other experiments to calculate the total number of simulated particles. For each isotope, the efficiency of the full-energy peak was employed.

Some experimental spectra did not align precisely with the anticipated source energies, differing by one energy bin. For the plots shown in the figure, this data was shifted. For Zn-65, we see an additional peak at 511 keV. The peak results from photons generated by the annihilation of positrons produced in the β^+ decay of Zn-65 (Karmalitsyn et al., 2004). Since OpenMC does not simulate this decay we initiated 511 keV photons according to the intensity of the β^+ decay.

Our simulation results generally agree well with the experimental gamma spectra in the sub-1 MeV range. For the spectra in the higher energy range, the simulation spectra are too strongly broadened, which is consistent with the fit in Fig. 8. In the low-energy regions of the spectra of Y-88, Zn-65, and Cs-137, we see X-ray peaks generated by surrounding materials. Since we only simulate a simple detector setup, these are not reproduced in our simulation results. We suspect that Au-198 was mixed with its metastable isomer in the experiments, which produces a gamma peak at 97 keV. In the case of Al-28 and Rb-86, we suspect some detector malfunction, like electronic noise in the lower energy region of the detector. A discrepancy is also evident in the Co-60 spectrum. The experimental data includes the summation peak of both photon energies, 1.17 MeV and 1.33 MeV. After the β^- decay, two photons with these energies are emitted in succession within picoseconds. A summation event occurs if the detector absorbs both photons. We have included the sum of the two energies in the figure as a purple dashed line. To simulate such effects with OpenMC (or MCNP), the software would need to initiate several photons for the same particle history. Both codes, however, lack such functionality. Two solutions could be implemented to achieve the summation peak. First, simulation results of individual particles are combined through post-processing after the Monte Carlo simulation. Li et al. (2016) demonstrates this for MCNP, a similar approach could be taken analogously for OpenMC calculations. Secondly, the software itself could be modified. In OpenMC, the `secondary_bank` could be used to start a second photon together with

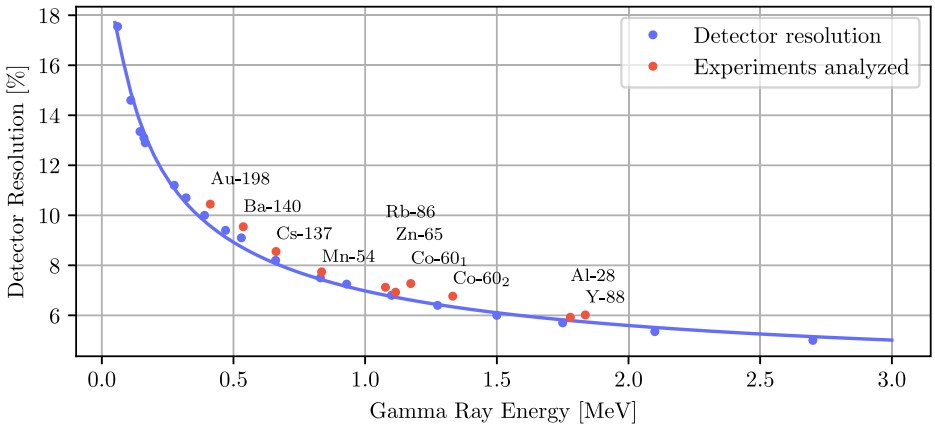

Fig. 8. Detector resolution. Blue dots show the values given in Heath (1964). The blue line corresponds to the fit parameters detailed in the text, while the red dots represent the resolution for the experimental spectra under consideration.

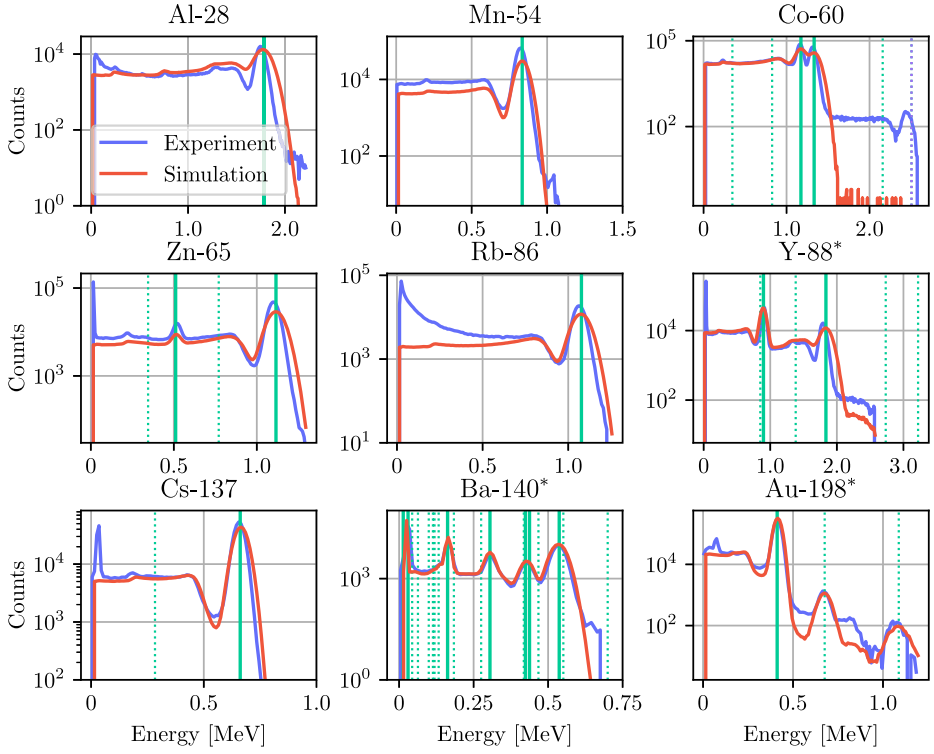

Fig. 9. Incorporate energy broadening according to the detector resolution. The energies of the initial source photons are indicated by green vertical lines, with dotted lines representing energy levels contributing less than one percent to the total intensity. * simulated spectrum has been normalized with the total counts of the experiment.

an initial particle. Both solutions are outside the scope of this article, as its primary focus is on the validation of the Pulse-Height Tally (PHT).

4. Conclusion and outlook

Although the Monte Carlo particle transport software OpenMC has the capability to simulate photons since several years, it lacked the functionality for detector simulations of gamma spectroscopy. This publication introduces a significant and novel extension to the software, a pulse-height tally function designed for photons. The rigorous validation tests described here demonstrate this new feature's robustness and accuracy, making it a valuable tool for various applications using different detector systems. Future improvements should address more complex scenarios, such as accounting for correlated particles from individual decay events and extending the tally to neutron applications.

Code availability

The PHT was added to the official OpenMC code starting with 0.13.4-dev. All input files, results of the simulations, and scripts for creating the plots are available on GitHub.[4]

CRediT authorship contribution statement

Christopher Fichtlscherer: Writing – review & editing, Writing – original draft, Visualization, Validation, Software, Methodology, Conceptualization. **Milon Miah:** Validation. **Friederike Frieß:** Writing –

[4] https://github.com/cfichtlscherer/Implementation_and_Validation_of_the_Pulse-Height_Tally_in_OpenMC_Code.

review & editing. **Malte Göttsche:** Writing – review & editing, Supervision. **Moritz Kütt:** Writing – review & editing, Writing – original draft, Validation, Supervision, Methodology, Conceptualization.

Declaration of competing interest

The authors declare that they have no known competing financial interests or personal relationships that could have appeared to influence the work reported in this paper.

Data availability

All input files, results of the simulations, and scripts for creating the plots are available on GitHub.

Acknowledgments

This work was supported by the German Foundation for Peace Research (DSF) through the research project "Nuclear Warhead Authentication Based on Gamma and Neutron Emissions - How to Discourage Cheating?" Malte Göttsche's contribution is supported by the Volkswagen Foundation, Germany. OpenMC simulations were performed using computing resources granted by RWTH Aachen University, Germany under project rwth0572. We thank the Institute of Nuclear Materials Management for permission to use previously presented figures (Figs. 1 and 5).

References

Agostinelli, S., Allison, J., Amako, K., Apostolakis, J., Araujo, H., Arce, P., Asai, M., Axen, D., Banerjee, S., Barrand, G., et al., 2003. Nucl. Instrum. Methods A 506, 250–303. http://dx.doi.org/10.1016/S0168-9002(03)01368-8.

Bates, C.R., Biondo, E., Huff, K., et al., 2014. Trans. Am. Nucl. Soc. 111, 1165–1168.

Böhlen, T.T., Cerutti, F., Chin, M.P.W., Fassò, A., Ferrari, A., Ortega, P.G., Mairani, A., Sala, P.R., Smirnov, G., Vlachoudis, V., 2014. Nucl. Data Sheets 120, 211–214. http://dx.doi.org/10.1016/j.nds.2014.07.049.

Boltzmann, L., 1872. Sitzungsber. Akad. Wiss. Vienna 66, 275–370.

Booth, T.E., 1994. Nucl. Sci. Eng. 116, 113–124. http://dx.doi.org/10.13182/NSE94-A21487.

Carasco, C., 2021. Nucl. Instrum. Methods A 990, 164985. http://dx.doi.org/10.1016/j.nima.2020.164985.

Carminati, M., Di Vita, D., Morandi, G., D'Adda, I., Fiorini, C., 2022. Sensors 22 (4), 1412. http://dx.doi.org/10.3390/s22041412.

Cullen, D.E., Hubbell, J.H., Kissel, L., 1997. Techn. Rep. UCRL-50400. http://dx.doi.org/10.2172/295438.

El-Bouzaidi, M.D., El Bardouni, T., El Hajjaji, O., Idrissi, A., Chham, E., Pérez, A.M., Mira, M., 2023. Rad. Phys. Chem. 206, 110777. http://dx.doi.org/10.1016/j.radphyschem.2023.110777.

Ferrari, A., Sala, P.R., Fasso, A., Ranft, J., 2005. FLUKA: A Multi-Particle Transport Code (Program Version 2005), first ed. CERN Yellow Reports, Geneva.

Fichtlscherer, C., Frieß, F., Göttsche, M., Kütt, M., 2021. Proc. INMM Ann. Meet..

Han, M.C., Pia, M.G., Saracco, P., Basaglia, T., 2018. IEEE Trans. Nucl. Sci. 65, 2268–2278. http://dx.doi.org/10.1109/TNS.2018.2849328.

Heath, R.L., 1964. Tech. Rep. IDO-16880-2. http://dx.doi.org/10.2172/4033555.

Hirayama, H., Namito, Y., Bielajew, A.F., Wilderman, S.J., Nelson, W.R., 2015. SLAC Rep. SLAC-R-730, KEK Report 2005-8.

Horne, S.M., Thoreson, G.G., Theisen, L.A., Mitchell, D.J., Harding, L., Amai, W.A., 2016. SAND2016-4345 639571. http://dx.doi.org/10.2172/1431293.

Jeon, J., Park, C.J., Kim, G., 2020. Nucl. Instrum. Methods A 954, 162302. http://dx.doi.org/10.1016/j.nima.2019.06.043.

Karmalitsyn, N.I., Sazonova, T.E., Sepman, S.V., Zanevsky, A.V., 2004. Appl. Radiat. Isot. 60, 391–395. http://dx.doi.org/10.1016/j.apradiso.2003.11.047.

Kawrakow, I., Mainegra-Hing, E., Rogers, D.W.O., Tessier, F., Walters, B.R.B., 2021. NRCC Report PIRS-701.

Knoll, G.F., 2010. Radiation Detection and Measurement, fourth ed. Wiley, Hoboken, New Jersey, pp. 322–366.

Kütt, M., Glaser, A., 2019. PLoS One 14 (10), e0224149. http://dx.doi.org/10.1371/journal.pone.0224149.

Li, L., Quincy, A., van der Ende, B., 2016. CNL Nucl. Rev. 6, 215–219. http://dx.doi.org/10.12943/CNR.2015.00053.

Lund, A.L., Romano, P.K., 2018. Tech. Rep. ANL/MCS-TM-381 149145. http://dx.doi.org/10.2172/1490825.

Massey, Jr., F.J., 1951. J. Amer. Statist. Assoc. 46, 68–78. http://dx.doi.org/10.2307/2280095.

Miah, M., 2022. Bach. Th. RWTH Aachen, Germany.

Mirion Technology Inc., Data Sheet CSP0232-02/09.

Nayak, S.S., Mukherjee, G., 2022. J. Instrum. 17, P07030. http://dx.doi.org/10.1088/1748-0221/17/07/P07030.

Nguyen, C.T., Zsigrai, J., 2006. Nucl. Instrum. Methods B 246 (2), 417–424. http://dx.doi.org/10.1016/j.nimb.2006.01.011.

2022. Openmc, LANL-based data libraries. https://openmc.org/lanl-data-libraries/ (accessed 14 March 2022).

Prettyman, T.H., Hagerty, J.J., Elphic, R.C., Feldman, W.C., Lawrence, D.J., McKinney, G.W., Vaniman, D.T., 2006. J. Geophys. Res. Planets 111 (E12), http://dx.doi.org/10.1029/2005JE002656.

Romano, P.K., Horelik, N.E., Herman, B.R., Nelson, A.G., Forget, B., Smith, K., 2015. Ann. Nucl. Energy 82, 90–97. http://dx.doi.org/10.1016/j.anucene.2014.07.048.

Saito, K., Moriuchi, S., 1981. Nucl. Instrum. Methods 185, 299–308. http://dx.doi.org/10.1016/0029-554X(81)91225-8.

Salvat, F., Fernandez-Varea, J.M., Sempau, J., 2009. PENELOPE-2008: A Code System for Monte Carlo Simulation of Electron and Photon Transport. OECD, NEA, No. 6416.

Scot, V., Fernandez, J.E., 2015. Spectrochim. Acta B 108, 53–60. http://dx.doi.org/10.1016/j.sab.2015.02.005.

Shuttleworth, T., 1994. Proc. Eighth I. Con. Rad. Shield.

Sood, A., Forster, R.A., Adams, B.J., White, M.C., 2004. Nucl. Instrum. Methods B 213, 167–171. http://dx.doi.org/10.1016/S0168-583X(03)01598-2.

Sood, A., Reed, M.S., Forster, R.A., 2003. Tech. Rep. la-UR-03-4271.

Tichacek, C.J., Budzevich, M.M., Wadas, T.J., Morse, D.L., Moros, E.G., 2019. Molecules 24, 3397. http://dx.doi.org/10.3390/molecules24183397.

Werner, C.J., Bull, J.S., et al., 2018. Tech. Rep. la-UR-18-20808. http://dx.doi.org/10.2172/1419730.